# Liquid-crystal anchoring transitions on aligning substrates processed by a plasma beam

Oleg V. Yaroshchuk,* Alexei D. Kiselev,† and Ruslan M. Kravchuk
*Institute of Physics of National Academy of Sciences of Ukraine, prospekt Nauki 46, 03028 Kyïv, Ukraine*
(Received 25 October 2007; revised manuscript received 29 January 2008; published 26 March 2008)

We have studied a sequence of anchoring transitions observed in nematic liquid crystals (NLCs) sandwiched between hydrophobic polyimide substrates treated with a plasma beam. There is a pronounced continuous transition from a homeotropic to a slightly tilted (nearly planar) alignment with the easy axis parallel to the incidence plane of the plasma beam (the zenithal transition) which takes place as the exposure dose increases. In NLCs with positive dielectric anisotropy, a further increase in the exposure dose results in in-plane reorientation of the easy axis by 90° (the azimuthal transition). This transition occurs through the twofold degenerate alignment characteristic of second-order anchoring transitions. In contrast to the critical behavior of anchoring, the contact angle of the NLC and water on the treated substrates declines monotonically with increasing exposure dose. It follows that the surface concentration of hydrophobic chains decreases continuously. The anchoring transitions under consideration are qualitatively interpreted by using a simple phenomenological model of competing easy axes which is studied by analyzing anchoring diagrams of generalized polar and nonpolar anchoring models.

DOI: 10.1103/PhysRevE.77.031706 PACS number(s): 61.30.Hn, 79.20.Rf, 78.66.Qn

## I. INTRODUCTION

The orientational structure of a nematic liquid crystal (NLC) placed in contact with an anisotropic substrate is essentially determined by the properties of the interfacial region, where various kinds of surface-induced ordering may exist. Among these are smectic layering, biaxiality, and orientational alignment (see, e.g., [1–3] for reviews).

At the macroscopic level, the surface-induced orientation of NLC molecules in the interfacial layer manifests itself as the well-known phenomenon of *anchoring*. In the case of uniaxial anisotropy, anchoring can be roughly described as the tendency of the nematic director **n** to align along the direction of preferential anchoring orientation at the surface. The direction of surface-induced alignment is specified by a unit vector $\mathbf{n}_s$ and is referred to as the *easy axis*.

Anchoring is governed by the so-called *anchoring energy* $W_{anch}$, which is the orientationally dependent (anisotropic) part of the surface tension. In particular, easy axes can be found by minimizing the anchoring potential and, thus, crucially depend on the shape of $W_{anch}$. When the anchoring energy changes, the easy axes may vary in both direction and number. Such variations of the anchoring conditions result in a reorientation of the NLC director known as the *anchoring (surface) transition* (AT).

Since the anchoring potential is sensitive to the thermodynamic parameters, anchoring transitions, like phase transitions, can be driven by temperature, chemical potential, and strain. They can also be first and second order depending on whether the anchoring-induced reorientation is discontinuous (jumplike) or continuous at the critical point. For planar interfaces, the transitions that occur through out-of-plane, in-plane, and mixed director reorientations may be classified as the *zenithal*, *azimuthal*, and *mixed* anchoring transitions, respectively.

For example, a discontinuous zenithal transition from planar to homeotropic orientation was found to occur on a flat glass or quartz substrate when it was cooled toward the smectic-*A* transition temperature [4], and on the surface of a self-assembled monolayer that was made sufficiently hydrophobic [5]. By contrast, the temperature-driven zenithal transitions observed at free NLC surface [6–8] and at rubbed polyimide aligning layers [9] turned out to be continuous.

Transitions between different anchorings can be generated by change in either the molecular characteristics of the NLC material or the parameters determining the structure of the substrate. The series of azimuthal anchoring transitions on the cleaved surfaces of some crystals such as gypsum and mica, studied in relation to the composition of water and alcohol vapors in the atmosphere above the nematic film [10–13], represent such transitions.

Of particular interest are the transitions governed by the parameters that characterize the method employed to treat the surface for fabrication of aligning films. A variety of photoinduced orientational surface transitions that were observed in [14–18] are related to the photoalignment technique, in which an aligning layer is irradiated with actinic light (see [19,20] for recent reviews).

Another approach suggested in [21,22] is to align liquid crystals with obliquely evaporated thin films of silicon oxide $SiO_x$. The anchoring of nematics at obliquely evaporated $SiO_x$ was studied as a function of the evaporation angle [23] and the film thickness [24]. It was found that an increase in either of these parameters may initiate a sequence of mixed and zenithal continuous surface transitions between three different anchorings: planar monostable, tilted bistable, and tilted monostable.

In this paper, we deal with anchoring transitions on substrates treated with ion or plasma beams. Recently, this kind of treatment has aroused considerable interest because it offers the greatest promise for replacing the traditional rubbing technique in the new generation of liquid crystal displays (LCDs) [25–27]. This processing avoids direct mechanical contact with the aligning substrates, thus minimizing the sur-

*olegyar@iop.kiev.ua
†kiselev@iop.kiev.ua

 

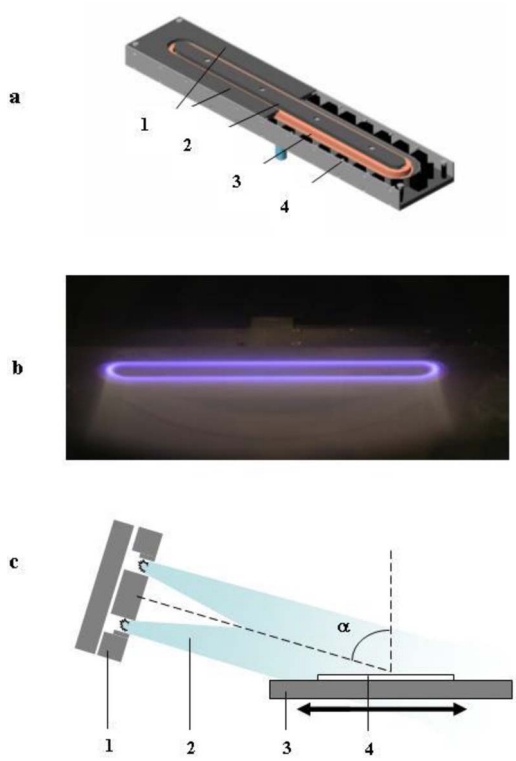


FIG. 1. (Color online) (a) Scheme of anode layer source: (1) inner cathode, (2) outer cathode, (3) anode, and (4) permanent magnets. (b) Glow discharge and beams of Ar plasma generated by anode layer source. (c) Geometry of plasma beam irradiation: (1) anode layer source, (2) sheetlike plasma flux, (3) moving platform, and (4) substrate.

face deterioration. It also provides highly uniform alignment on microscopic and macroscopic scales with pretilt angle and anchoring energy controlled in a wide range. We apply this method to treat films of hydrophobic polyimide and investigate the anchoring transitions at the plasma-modified substrates as a function of the irradiation dose.

The layout of the paper is as follows. The experimental procedure is described in Sec. II. We present our results in Sec. III and, in Sec. IV, discuss how they can be interpreted theoretically using a phenomenological model of two competing easy axes with the anchoring potential taken in the Sen-Sullivan form [28]. Concluding remarks are given in Sec. V.

## II. EXPERIMENT

### A. Setup for plasma beam exposure

The irradiation setup was based on an anode layer source (ALS) from the Hall family of sources working in the beam mode [29]. The general construction of this source is presented in Fig. 1(a). A glow discharge is initiated in the crossed electric and magnetic fields within the discharge channel formed by the inner and outer cathodes and the anode. Because of the high anode potential, the ions of the plasma are pushed out of the discharge area. They involve electrons so that the beam of accelerated plasma is formed. In contrast to the Kaufman source widely used for ion beam alignment processing [25,30], the ALS does not contain any grids or hot elements (such as filaments and other secondary electron sources). The structure is thus simple and allows one to substantially increase reliability.

We used the ALS with a racetrack-shaped glow discharge so that the source generates two "sheets" of accelerated plasma [Fig. 1(b)]. As we have shown previously, this construction is very well suited for the alignment treatment of large-area substrates: if the substrate is moved across the plasma sheet, the only limiting factor for the width of this substrate is the width of the sheet. Since the ALS can be easily scaled up, this process can be extended for the alignment treatment of large-area substrates used in modern LCD industry.

The feed gas was argon. The working pressure $P$ in our experiments was $1.4\times10^{-4}$ Torr which corresponded to a current density $j$ within the beam of 0.4 $\mu$A cm$^{-2}$. The low current was used to gradually vary the exposure dose, given by the product of the current density and the exposure (treatment) time $\tau_{\mathrm{exp}}$. The anode potential $U$ determining the maximum energy of the plasma $Ar^+$ ions was 600 V.

The geometry of exposure is shown in Fig. 1(c). The substrates were irradiated obliquely and the incidence angle of the plasma beam, $\alpha$, was about 75°. The substrate's holder was mounted on a PC-controlled translator in a vacuum chamber under the discharge channel. The substrates were treated in both the dynamic and static regimes. Different parts of the sample were passed through the plasma beam many times, undergoing alignment treatment repeatedly (the cycling regime of treatment), so that alignment uniformity was substantially improved. The approximate distance between the plasma outlet and the substrate of size of $20\times30$ mm$^2$ was 8 cm.

### B. Samples and their characterization

We used a fluorinated polyimide (PI-F) containing hydrophobic side chains as a polymer material. The polymer was dissolved in an appropriate solvent and spin coated on a glass plate over indium tin oxide (ITO) electrodes. The substrates were then baked at 180 °C over 1.5 h to remove the solvent.

Two types of NLC cells were prepared: (1) identical substrates with the plasma-treated PI-F films were assembled to form symmetric NLC cells with antiparallel director orientation; (2) the tested substrate with the plasma-modified PI-F layer and a reference substrate with a rubbed polyimide (9203 from JSR) layer were arranged so as to form asymmetric NLC cells where the rubbing direction was antiparallel to the direction of plasma irradiation. In both cases the cell thickness was kept at 20 $\mu$m.

The symmetric cells were used to measure the pretilt angle of the NLC by the crystal rotation method, whereas the asymmetric cells served to determine the in-plane direction of the easy axis. The NLCs K15 [n-pently-n'-cyanbiphenyl (5CB)] from Merck and MJ961180 from Merck Japan in an isotropic phase were injected into the cells by capillary ac-

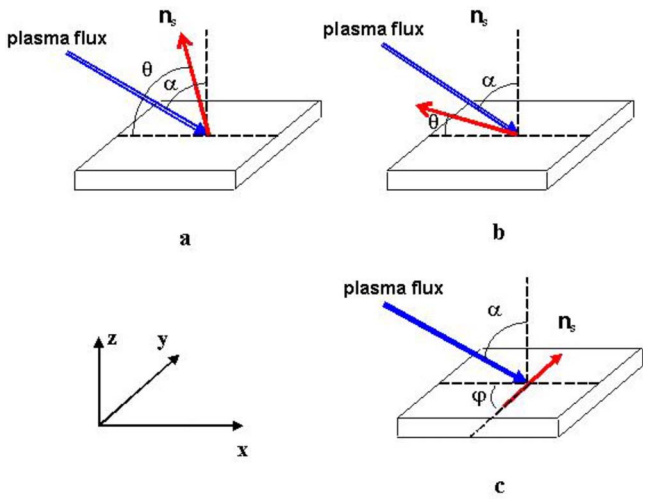


FIG. 2. (Color online) Types of NLC alignment observed in our experiments: (a) slightly tilted (nearly homeotropic) structure (alignment of the first type with $75° \leq \theta \leq 90°$ and $\phi = 0°$); (b) highly tilted (nearly planar) structure (alignment of the second type with $0° \leq \theta \leq 30°$ and $\phi = 0°$) which is close to planar anchoring; and (c) planar anchoring normal to the incidence (the $x$-$z$) plane (alignment of the third type with $\theta = 0°$ and $\phi = 90°$).

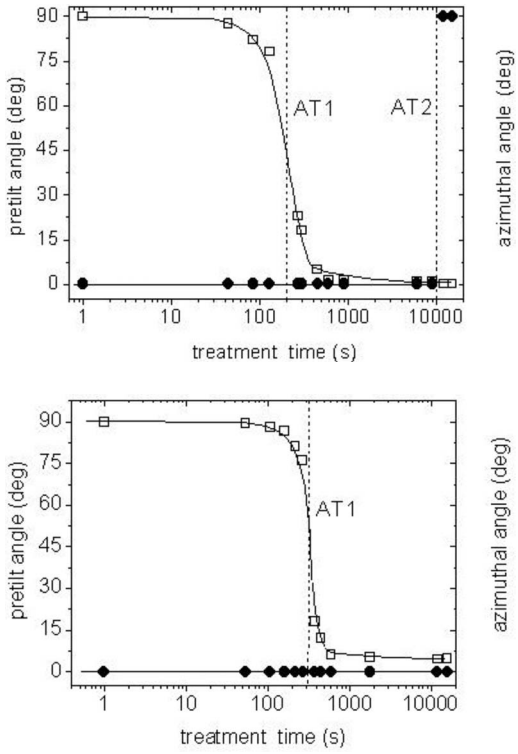


FIG. 3. Pretilt angle $\theta$ (open squares) and azimuthal angle $\phi$ (filled circles) measured as a function of the treatment (exposure) time in the LCs 5CB (a) and MJ961180 (b) at plasma-modified PI-F substrates. Treatment conditions are $\alpha = 75°$, j=0.4 $\mu$A cm$^{-2}$, $U = 600$ V. Zenithal and azimuthal anchoring transitions are marked AT1 and AT2, respectively.

tion. The LC 5CB with positive dielectric anisotropy $\Delta\varepsilon$ is a well-characterized nematic cyanobiphenyl used as a component of industrial twisted nematic (TN) LC mixtures. The mixture LC MJ961180 with $\Delta\varepsilon < 0$ is developed for vertically aligned (VA) LCD. The quality of sample alignment was judged by observation in a polarizing microscope and with the naked eye by placing a sample between crossed polarizers.

## III. RESULTS

The orientation of the easy axis induced by the plasma beam processing is specified by the pretilt and azimuthal angles $\theta$ and $\phi$ (see Fig. 2). Figures 3(a) and 3(b) show these angles measured as a function of the exposure time in the cells filled with the LC 5CB and the LC mixture MJ961180, respectively.

For the 5CB cells, the curves indicate a pronounced homeotropic-to-oblique anchoring transition that occurs at low irradiation dose. In this case, the easy axis initially directed along the normal to the substrate (the $z$ axis) inclines continuously in the incidence plane of the plasma beam (the $x$-$z$ plane) toward the plasma beam direction (Fig. 2). When the exposure time $\tau_{exp}$ is increased, the pretilt angle first decreases gradually from 90° to 75°. The angle declines steeply to $\theta \approx 25°$ at the critical point. Then it decays to a value of about 2° which changes weakly with the exposure time.

From the dependence of the azimuthal angle on the irradiation time plotted in Fig. 3(a), it can be inferred that the above zenithal transition (AT1) is followed by an azimuthal transition (AT2) which takes place in the region of long-time treatment. In this case the result of drastic in-plane reorientation is that the easy axis lying initially in the plane of incidence is rotated through 90°. Thus, we have a transition between two planar anchorings: $\mathbf{n}_s = \hat{\mathbf{x}}$ and $\mathbf{n}_s = \hat{\mathbf{y}}$ (see Fig. 2).

So the results for the LC 5CB representing nematic materials of positive dielectric anisotropy clearly indicate two anchoring transitions driven by the irradiation dose: zenithal and azimuthal. The sequence of transitions involves three different anchorings that can be described as three types of LC alignment: (1) a highly tilted structure (nearly homeotropic) with zero azimuthal angle (alignment of the first type) observed in the region of low irradiation doses before the zenithal transition; (2) a slightly tilted structure (nearly planar) with zero azimuthal angle (alignment of the second type) observed between the anchoring transitions; (3) planar anchoring with the easy axis normal to the incidence plane (alignment of the third type) detected above the critical dose of the azimuthal transition. Figure 4 shows that the alignment of the above listed orientational structures is of excellent quality.

The curves presented in Fig. 3(b) were measured in the cells filled with the LC mixture MJ961180, which is a nematic material with negative dielectric anisotropy, $\Delta\varepsilon < 0$. It can be seen that, as far as the zenithal transition is concerned, the results for this mixture are quite similar to those obtained for 5CB cells. Quantitatively, as opposed to the LC 5CB, the pretilt angle above the critical point remains approximately constant, varying in the range between 30° and 15°. The

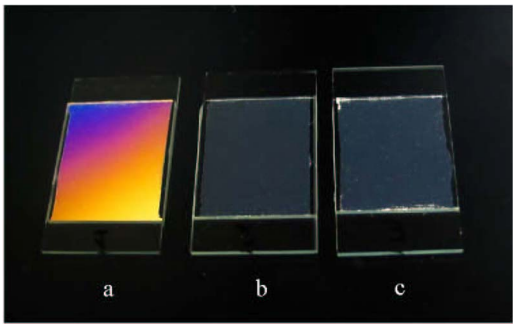


FIG. 4. (Color online) Symmetric antiparallel cells filled with LC 5CB and viewed between a pair of crossed polarizers from an oblique direction. The polarizer at the bottom is aligned vertically. The PI-F substrates are treated with the plasma beam for 40 (a), 1000 (b) and 15 000 (c) s. Projection of the plasma beam onto the substrate (the $x$ axis) is parallel to its long side. The cells demonstrate three different types of alignment: (a) highly tilted, (b) slightly tilted, and (c) planar, respectively. Treatment conditions are $\alpha=75°$, j=0.4 $\mu$A cm$^{-2}$, $U=600$ V.

most important difference is that the azimuthal anchoring transition with in-plane reorientation toward the normal of the incidence plane turned out to be suppressed.

The experimental data presented in Fig. 3(a) are insufficient to judge the character of the azimuthal anchoring transition unambiguously. In order to clarify the behavior of anchoring near the critical point AT2, we used the substrates treated in the static regime of irradiation. Since the beam profile in the transverse direction has Gaussian shape, the exposure dose appears to be continuously distributed over the substrate area.

In Fig. 5, the sample as viewed between differently aligned polarizers is presented for a typical asymmetric 5CB cell with the PI-F substrate processed in the static regime with only one plasma sheet. It can be concluded that, in the central part (part $A$) of the cell exposed to the highest dose with the maximum intensity, anchoring is planar with the director normal to the incidence plane (alignment of the third type). By contrast, the periphery (part $B$) of the cell is characterized by planar alignment of the second type (the easy axis is parallel to the plane of incidence).

There are two transient striplike regions between the parts of low and high irradiation doses shown in Fig. 5 as parts $C$ and $C'$. These regions are divided into narrow domains. Owing to the mirror symmetry, any two domains oriented symmetrically with respect to the plane of incidence are equiprobable provided that the irradiation dose is fixed.

The strips are found to differ in width. As is illustrated in Fig. 6, there are two parts of the plasma flux with intensities in the interval $[j_t, j_t+\Delta j_t]$ that induce the transient alignment $C$. These parts are projected onto the alignment substrate at different incidence angles so that the strip that is closer to the source is narrower than the other one.

From Fig. 5, the strips $C$ and $C'$ are both rather narrow. This means that the beam intensity is tightly distributed over the range $[j_t, j_t+\Delta j_t]$. Hence, the production of a substrate aligned like this strip in the dynamic regime of irradiation can be rather difficult as it requires using a fine-tuning procedure for the irradiation doses.

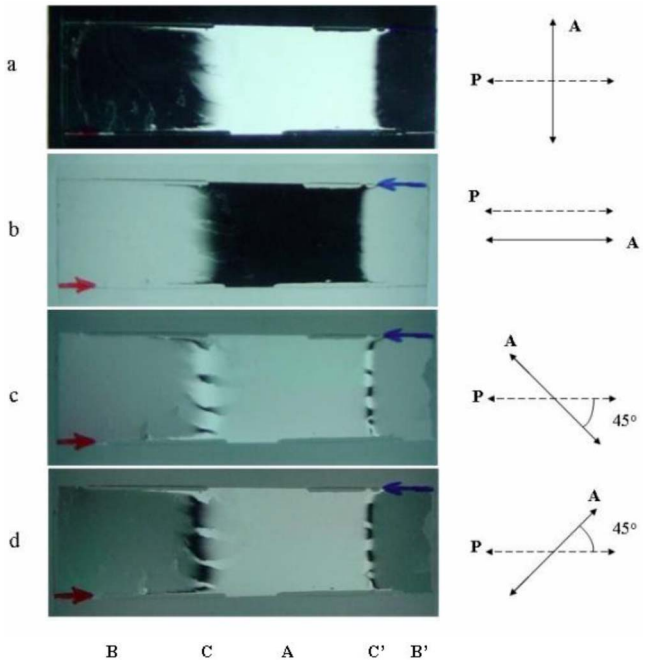


FIG. 5. (Color online) Photos of asymmetric cell viewed between the horizontally aligned polarizer and the analyzer oriented at four different angles (a) 90°; (b) 0°; (c) +45°; (d) −45°. The reference (bottom) substrate is the rubbed PI film, whereas the tested (upper) substrate is the PI-F layer treated in the static regime with one plasma sheet ($\alpha=60°$, j=4.5 $\mu$A cm$^{-2}$, $U=600$ V, $\tau_{exp}=11$ min). The arrows on the left- and right-hand sides of the figure indicate the directions of rubbing and of the plasma beam, respectively. These are arranged to be antiparallel. In the central part of the tested substrate (part $A$) exposed to the central part of the plasma sheet having maximum intensity, NLC alignment corresponds to planar anchoring with the easy axis normal to the incidence plane (alignment of the third type). In periphery parts subjected to low irradiation doses (parts $B$ and $B'$), the easy axis of planar anchoring lies in the plane of incidence (alignment of the second type). These parts are separated by planar-oriented strips (parts $C$ and $C'$) of transient twofold-degenerate alignment.

## IV. DISCUSSION

We can now take a closer look at the properties of the anchoring transitions described in the previous section. Our first remarks concern the character of the transitions.

In our experiments, the irradiation-dose-driven zenithal transition was found to take place in the plane of incidence for either sign of the NLC dielectric anisotropy. When the dose is increased, the transition occurs through homeotropic to (nearly) planar reorientation of the easy axis and manifests itself as a steep decline of the pretilt angle in the immediate vicinity of the critical dose (see the curves in Fig. 3). Since the reorientation does not show any discontinuities, it may be concluded that the transition is second order. Transitions of this type were previously obtained on films modified with actinic light [15,16] and cold plasma [31–33].

The anchoring is monostable and planar in 5CB cells treated for so long that irradiation doses are well beyond the critical point of the homeotropic-to-planar transition. As can

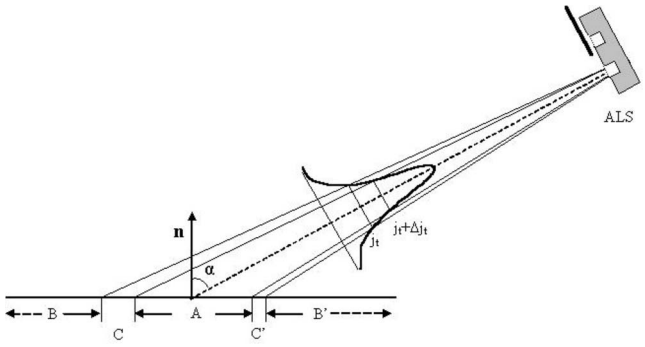


FIG. 6. Scheme illustrating irradiation in the static regime and corresponding types of LC alignment. One linear part of the discharge slot is closed so as to select only one plasma sheet. The transverse intensity distribution of this sheet is of Gaussian shape. Given the exposure time, the beam intensities $j_2 < j_t$ and $j_3 > j_t + \Delta j_t$ are shown to correspond to the second (parts $B$ and $B'$) and the third (part $A$) alignment types, respectively. For intensities ranging between $j_t$ and $j_t + \Delta j_t$, transient alignment is observed (parts $C$ and $C'$). The strips $C$ and $C'$ are of different widths because the upper and lower fractions of the beam with intensities in the interval $[j_t, j_t + \Delta j_t]$ are projected onto the substrate at different incidence angles.

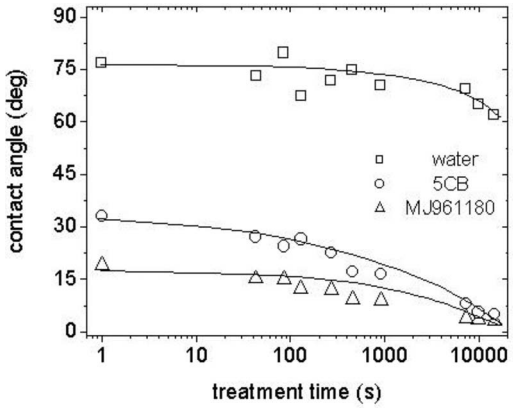


FIG. 7. Contact angle as a function of the exposure time for droplets of LC 5CB (circles), LC MJ961180 (triangles), and distilled water (squares) spread upon plasma-treated PI-F substrates. Treatment conditions are $\alpha = 75°$, j=0.4 $\mu$A cm$^{-2}$, $U = 600$ V.

be seen from Fig. 3(a), the curve for the azimuthal angle suggests that the zenithal transition, AT1, is followed by the azimuthal one, AT2.

This is the transition between two planar anchorings in which the easy axis is either parallel or normal to the incidence plane (the $x$-$z$ plane). It is characterized by in-plane reorientation of the director, which is rotated abruptly by 90° near the critical point.

But the image of the asymmetric cell with one of the substrates treated in the static regime (see Fig. 5) clearly shows the presence of planar oriented domains where the director is tilted with respect to the plane of incidence. Such strips of transient alignment are typical of second-order transitions where fluctuations create domains having close orientations [2,13]. Transitions of similar character were generated at obliquely evaporated $SiO_x$ films [23,24] and at photoaligned layers [17].

The changes of anchoring direction are caused by surface modification of the aligning films induced by plasma beam treatment. By analogy with other plasma processes [31,33], the plasma beam may destroy hydrophobic side chains and increase the free energy of the aligning layer.

Gradual reduction of hydrophobic chains on the polymer surface was directly detected by x-ray photoelectron spectroscopy (XPS) in [31]. We carried out contact angle measurements which, according to [34], can be used to obtain indirect experimental evidence that the hydrophobic chain concentration diminishes with increasing exposure dose.

Figure 7 presents the contact angle as a function of the exposure time measured at room temperature for three kinds of material: the LCs 5CB and MJ961180 and distilled water. It is clear that, for all compounds, the contact angle gradually declines with increasing exposure dose. This means that surface hydrophobicity decreases monotonically, whereas the surface free energy increases. In contrast to the NLC alignment, the contact angles do not reveal any signs of critical behavior at the exposure doses corresponding to AT1 and AT2.

It is reasonable to assume that a critical concentration of hydrophobic chains should be reached to trigger the zenithal anchoring transition. This concentration is associated with the critical value of the surface free energy.

The mechanisms behind the azimuthal anchoring transition in 5CB cells are much less clear. Our assumption is that it is governed by topography factors. Our previous results [26,27] suggest that the plasma beam may produce anisotropy of the surface relief. In addition, microgrooves generated by the plasma beam from the ALS were recently detected in [35]. With increasing exposure dose, the topographical anisotropy changes direction from the direction of projection of the plasma beam on the substrate to the perpendicular direction.

This might explain the azimuthal transition from the second to the third type of alignment for the LC 5CB. This anchoring transition seems to be possible only if the pretilt angle is sufficiently low, whereas the topography factor is of minor importance at high pretilt angles.

Interestingly, our results concerning materials of different signs of the dielectric anisotropy bear close similarity to those reported in Ref. [36], where orientation of NLCs with positive (E8) and negative (MLC 95–465) dielectric anisotropy on obliquely evaporated $SiO_2$ films in relation to the evaporation angle $\alpha$ was studied experimentally. For E8, alignment is planar (and perpendicular to the incidence plane) at sufficiently small evaporation angles ($\alpha < 60°$), whereas, for $\alpha > 60°$, the alignment is tilted in the incidence plane. By contrast, for $\Delta\varepsilon < 0$, the director remains in the plane of incidence and the alignment approaches a homeotropic structure as the evaporation angle decreases. The different alignment behavior of the NLC materials is attributed to the van der Waals (VdW) interaction and order electricity . The competing effects between the VdW and dipole-to-dipole interactions are considered in [37] to explain why vertical alignment of NLC with negative dielectric aniso-

tropy on both $SiO_x$ and PI can be improved by doping with a positive dielectric material such as 5CB.

In closing this section, we discuss a simple phenomenological model that can be used to describe both the zenithal and azimuthal anchoring transitions qualitatively. Typically, such models are formulated in terms of phenomenological expressions for the anchoring energy potential. So the orientational structure in a uniformly aligned NLC cell is determined by the easy axis, which can be computed by minimizing the anchoring energy.

First we consider the most extensively studied case of isotropic flat substrates where the symmetry of the surface is characterized by its normal, $\hat{\mathbf{k}}=\hat{\mathbf{z}}$. So, the anchoring energy can be written as a function of the pretilt angle $\theta$ in the following generalized form:

$$W_{\mathrm{P}}(c) = w_1 c + \frac{w_2}{2}c^2 + \frac{w_4}{4}c^4, \tag{1}$$

where $c \equiv n_z = \sin\theta$ is the $z$ component of the NLC director $\mathbf{n}$. At $w_1 = w_4 = 0$, the energy (1) simplifies to the well known Papini-Papoular potential [38,39].

The first term on the right-hand side of Eq. (1) breaks equivalence between $\mathbf{n}$ and $-\mathbf{n}$ due to polar ordering effects in the interfacial layer [40,41]. A model with this polarity-breaking term and $w_4=0$ (Parson's model) was previously employed to describe anchoring transitions on oxidized silane substrates [31,32] and in freely suspended nematic films [8].

The expression for the anchoring energy with the positive fourth-order coefficient $w_4$ coming from the quadrupole-quadrupole interactions and short-range anisotropic repulsive and attractive forces [42–44] was originally derived by Sen and Sullivan [28]. A nonpolar azimuthally degenerate anchoring energy (1) with a quartic term ($w_1=0$ and $w_4 \neq 0$) was recently used to analyze temperature-driven transitions between the conical, planar, and anticonical anchorings observed on a grafted polymer brush [45].

The anchoring properties of the generalized potential (1) can be conveniently characterized by the anchoring phase diagram in the $w_2$-$w_4$ parameter plane. We present the phase anchoring diagrams for two cases: (a) the nonpolar model in the Sen-Sullivan form with $w_1=0$ (see Fig. 8) and (b) the generalized polar model with $w_1 \neq 0$ (see Fig. 9).

Referring to Fig. 8, when $w_1=0$ and the fourth-order (quartic) coefficient $w_4$ is positive, the regions of homeotropic (**N**), tilted (**T**), and planar anchorings (**P**), are separated by two solid lines $L_2$ and $w_2=0$, where the second-order transitions take place. More generally, the symbol **N** (**P**) marks regions where the easy axis is normal (parallel) to a specified reference plane such as the plane of the substrate or the incidence plane.

By contrast, if $w_4$ is negative, the transition between planar and homeotropic structures is discontinuous and does not involve tilted configurations. The structures are of the same energy at the points on the dashed line $L_1$.

In the coexistence regions $\mathbf{N}_B$ and $\mathbf{P}_B$, enclosed by the dash-dotted lines $L_2'$ and $w_2=0$, there is an energy barrier between the homeotropic and planar anchorings. According to Ref. [45], the latter can be referred to as anticonical anchoring. Note that the above results were previously reported for differently parametrized anchoring potentials in [42,45].

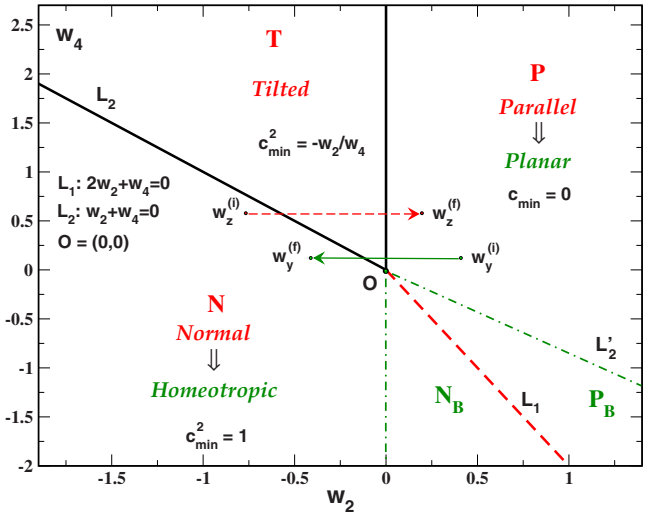


FIG. 8. (Color online) Anchoring phase diagram in the $w_2$-$w_4$ plane for the nonpolar potential (1) with $w_1=0$. Solid and dashed lines represent continuous and discontinuous transitions, respectively. The subscript $B$ identifies the regions where the homeotropic and planar structures are separated by the energy barrier.

In Fig. 9 we show the anchoring diagram for the less familiar case of the generalized model with nonvanishing polar coefficient $w_1$. The diagram does not depend on the sign of the polar coefficient because the potential (1) is invariant under the symmetry transformation $c \to -c$ and $w_1 \to -w_1$.

For $w_4 > -|w_1|/2$, as for the nonpolar model, the solid line $L_2$ defines the second-order transition between the homeotro-

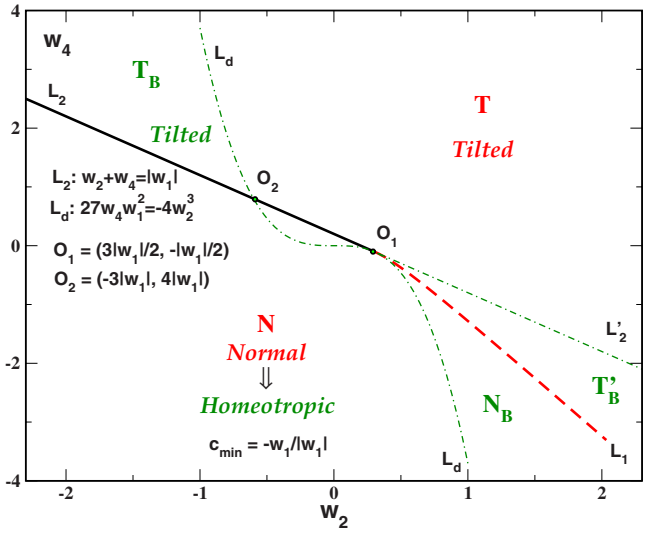


FIG. 9. (Color online) Anchoring phase diagram in the $w_2$-$w_4$ plane for the potential (1) in the presence of a polar term proportional to $w_1 \neq 0$. There is a metastable state separated from the equilibrium structure by an energy barrier in the regions labeled by subscript $B$. The special case where the metastable state corresponds to the homeotropic anchoring is marked by a prime.

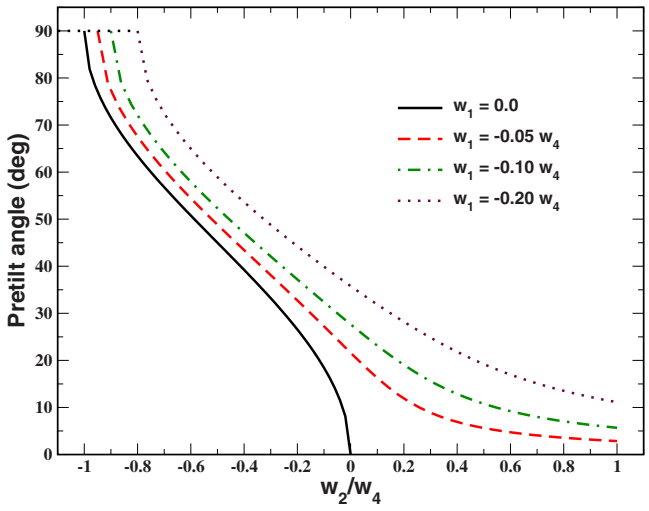


FIG. 10. (Color online) Pretilt angle versus the dimensionless anchoring parameter $w_2/w_4$ at different values of the polar coefficient $w_1$ for $w_4>0$.

pic and tilted structures. In contrast, the second-order transition between tilted and planar anchorings is suppressed as there are no regions of planar anchoring at $w_1 \neq 0$. From Fig. 9 this transition appears to be replaced by a crossing of the boundary curve $L_d$ between the regions $\mathbf{T}_B$ and $\mathbf{T}$ (the dash-dotted line $L_d$ above the point $O_2$). So the anchoring in the region $\mathbf{T}$ characterized by the tilted equilibrium structure and the absence of metastable states can be regarded as a counterpart of the planar structure (region $\mathbf{P}$ in Fig. 8).

In Fig. 9, the line corresponding to the first-order transition is depicted as the dashed curve $L_1$. The latter can be derived in the following parametrized form:

$$L_1 = \begin{cases} w_2 = |w_1|t^{-1}[1 + 2t^2(1+t)^{-2}], \\ w_4 = -2|w_1|t^{-1}(1+t)^{-2}, \end{cases} \tag{2}$$

where the parameter $t$, $0<t\leq 1$, defines the tilted configuration, $c_{\mathrm{tlt}}=-tw_1/|w_1|$, which is energetically equivalent to the homeotropic structure: $W_P(c_{\mathrm{tlt}})=W_P(c_{\mathrm{hom}})$ at $c_{\mathrm{hom}}=-w_1/|w_1|$.

It is clear that both the polar and nonpolar models predict anchoring transitions that can be either continuous or discontinuous depending on the value of the fourth-order coefficient $w_4$. It turned out that suppressing the planar anchoring is one of the most crucial effects induced by the polar term proportional to $w_1$. This effect can also be seen from the curves for the pretilt angle presented in Fig. 10 and computed as a function of the dimensionless parameter $\tilde{w}_2 \equiv w_2/w_4$ at a fixed ratio of $w_1$ and $w_4$.

The model (1) is azimuthally degenerate and thus cannot be applied directly to the transitions observed in our experiments. The important point is that the incidence plane of irradiation with the normal directed along the $y$ axis (see Fig. 2) has to be taken into account as an additional element of the surface geometry.

By the same reasoning as for obliquely evaporated $SiO_x$ [46], we find, on symmetry grounds, that the anchoring potential may additionally depend on $n_y^2$ and the model (1) can be extended as follows:

$$W = W_z(n_z) + W_y(n_y),$$

$$W_a(n_a) = \frac{w_2^{(a)}}{2}n_a^2 + \frac{w_4^{(a)}}{4}n_a^4, \quad a \in \{z,y\}. \tag{3}$$

Note that the polarity-breaking terms are neglected in the energy (3), so as not to rule out experimentally observed planar anchoring and structures tilted in the plane of incidence.

Generally, the $n_y$-dependent terms in the extended model arise from the reduction of symmetry caused by anisotropy of the substrate. In particular, under certain conditions, the energy (3) can be derived from the anchoring potential obtained in [47] for azo-dye photoaligned films.

The structure of the expression (3) bears close resemblance to models formulated in terms of two competing anchoring directions (easy axes). In the Rapini-Papoular approximation, such dual-axis models were previously employed to describe light-induced anchoring transitions in [16] and to study competitive effects of photoalignment and microgrooves in [48]. The anchoring properties of rubbed polyimide alignment layers were also studied by using the model supplemented with the fourth-order term in [9,49].

For the model (3), the anchoring transitions can be geometrically described in terms of two points: $\mathbf{w}_z \equiv (w_2^{(z)}, w_4^{(z)})$ and $\mathbf{w}_y \equiv (w_2^{(y)}, w_4^{(y)})$, so that the plane of reference is the substrate and the incidence plane for $\mathbf{w}_z$ and $\mathbf{w}_y$, respectively. These points both lie in the $w_2$-$w_4$ plane and the dependence of the anchoring coefficients at $\mathbf{w}_z$ and $\mathbf{w}_y$ on the irradiation dose can be depicted as two trajectories. The trajectories are illustrated in Fig. 8 under the simplifying assumption that the fourth-order coefficients $w_4^{(z)}$ and $w_4^{(y)}$ are kept constant and are independent of the treatment time.

The continuous homeotropic-to-planar transition occurs when the point $\mathbf{w}_z$ moves from its initial position in the region of homeotropic anchoring, $\mathbf{w}_z^{(i)} \in \mathbf{N}$, to the final state of planar anchoring with $\mathbf{w}_z^{(f)} \in \mathbf{P}$ through the region of tilted structures, $\mathbf{T}$. Reorientation of the director takes place in the incidence ($x$-$z$) plane provided $\mathbf{w}_y$ stays in the region $\mathbf{P}$ during the zenithal transition.

If $\mathbf{w}_z$ is in the region $\mathbf{P}$, anchoring is planar and the director orientation is determined by the position of the point $\mathbf{w}_y$. The azimuthal transition between planar structures aligned parallel ($n_y=0$) and normal ($n_y^2=1$) to the incidence plane can be depicted as the line connecting two points, $\mathbf{w}_y^{(i)} \in \mathbf{P}$ and $\mathbf{w}_y^{(f)} \in \mathbf{N}$ (see Fig. 8).

Now we demonstrate that the zenithal anchoring transition can be described quantitatively. For this purpose we take the assumption of exponential dependence of the anchoring coefficients $w_2^{(z)}$ and $w_4^{(z)}$ on the exposure time. On this assumption, the simplest analytical relation for the pretilt angle $\theta$ can be written in the following form:

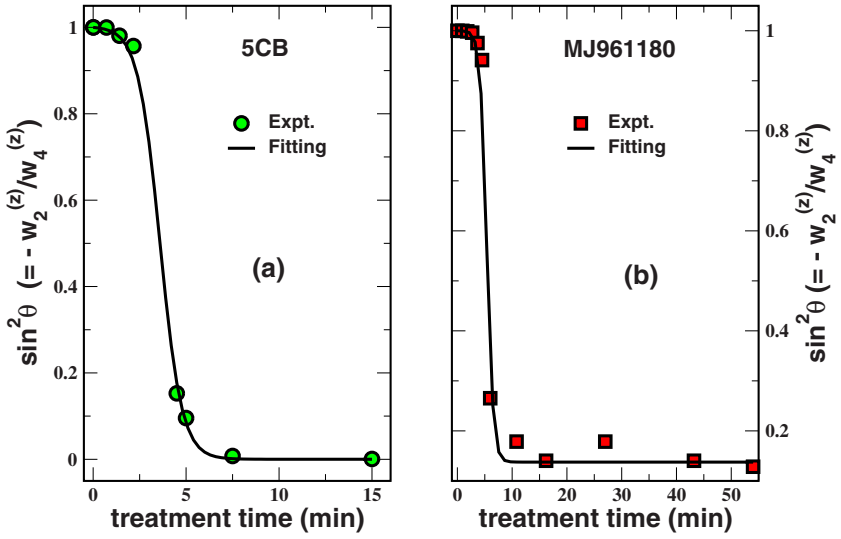


FIG. 11. (Color online) Anchoring parameter $-w_2/w_4$ ($=\sin^2\theta$) as a function of the treatment time measured in (a) 5CB and (b) MJ961180 cells. Experimental data are fitted using the formula (4) at $\gamma=1.7\ \mathrm{min}^{-1}$. The curves shown as solid lines are computed with the following dimensionless fitting parameters: (a) $\beta_4\approx 2.78\times 10^{-7}$ and $\beta_2\approx 2.21\times 10^{-3}$; (b) $\beta_4\approx 1.52\times 10^{-5}$ and $\beta_2\approx 1.1\times 10^{-4}$.

$$\sin^2\theta = -\frac{w_2^{(z)}}{w_4^{(z)}} = \frac{1+\beta_4[\exp(\gamma\tau_{\mathrm{exp}})-1]}{1+\beta_2[\exp(\gamma\tau_{\mathrm{exp}})-1]}, \tag{4}$$

where $\tau_{\mathrm{exp}}$ is the exposure (treatment) time. The results of phenomenological models for different photo-oriented films [50–52] and for aligning layers produced by collimated ion beams [25] both suggest that the exponential dependence is typical for the corresponding concentrations. So, in our case, it can be regarded as a reasonable approximation for the concentration of hydrophobic chains. Note that, strictly speaking, computing the pretilt angle requires a rather involved theoretical analysis which is beyond the scope of this paper.

The expression (4) can be used to fit the experimental data for the 5CB and MJ961180 cells. The results of the calculations are presented in Fig. 11. Clearly, they show that the difference between the materials is determined by the two fitting parameters $\beta_4$ and $\beta_2$. In particular, for 5CB cells, the ratio $\beta_4/\beta_2$ appears to be negligibly small and, as a result, the fourth-order coefficient $w_4^{(z)}$ is almost independent of the irradiation dose. (When the parameters $\gamma$, $\beta_4$, and $\beta_2$ are positive, the formula (4) implies that $-w_2^{(z)}\propto\{1+\beta_2[\exp(\gamma\tau_{\mathrm{exp}})-1]\}^{-1}$ and $w_4^{(z)}\propto\{1+\beta_4[\exp(\gamma\tau_{\mathrm{exp}})-1]\}^{-1}$.) But this is not the case for MJ961180 cells.

So, the experimentally observed transitions can be modeled by using the phenomenological anchoring potential (3). Note that, in the strict sense, our experiments do not imply that polar anchoring terms proportional to $w_1^{(z)}$ and $w_1^{(y)}$ are identically absent for all exposure doses. We can conclude only that the coefficient $w_1^{(z)}$ is negligible for 5CB cells at high irradiation doses in the region of planar anchorings, whereas the coefficient $w_1^{(y)}$ is zero during reorientation in the plane of incidence.

Interestingly, the model (3) can also be applied to the temperature-induced anchoring transition on a $SiO_x$ surface [46]. It can be shown that, when $w_2^{(y)}$ varies from $-w_4^{(y)}$ to zero lying on the line

$$\frac{w_2^{(z)}}{w_4^{(z)}} + \sin^2\alpha\left(\frac{w_2^{(y)}}{w_4^{(y)}}+1\right) = 0, \tag{5}$$

the anchoring changes from planar, $\mathbf{n}=(0,1,0)$, to tilted, $\mathbf{n}=(\cos\alpha,0,\sin\alpha)$, with the director moving on a plane that forms the angle $\alpha$ with the film. Qualitatively, this reproduces the behavior of the NLC director in the course of mixed anchoring transitions on obliquely evaporated $SiO_x$ films.

## V. CONCLUSIONS

We have observed experimentally second-order zenithal anchoring transitions in liquid crystals with positive and negative dielectric anisotropy oriented by hydrophobic substrates obliquely processed with a plasma beam. The transition is characterized by a pronounced decline of the pretilt angle with increasing exposure dose upon reaching the critical value of surface free energy related to the critical concentration of hydrophobic chains at the surface.

In the LC 5CB with $\Delta\varepsilon>0$, the zenithal transition is followed by the azimuthal transition when the exposure dose increases further. It occurs through the in-plane reorientation of the easy axis which is rotated by a right angle. This reorientation is found to involve twofold-degenerate transient structures and, as a consequence, we arrive at the conclusion that the azimuthal transition is second order. This transition can be reasonably explained by an experimentally detected change of the topographical anisotropy.

We have formulated a simple phenomenological model where two competing anchoring directions appear as a result

of additional plasma-beam-induced anisotropy of the treated substrate. In order to perform qualitative analysis of this model, the anchoring diagrams of the generalized potential were studied for both polar and nonpolar cases. The result is that the experimentally observed anchoring transitions can be properly modeled using the nonpolar dual-axis model supplemented with fourth-order terms.

In conclusion, it should be noted that all types of LC alignment observed in our experiments, such as high- and low-pretilt-angle structures along with planar alignment, are of considerable interest for applications. The technology-related issues were briefly discussed in our previous publications [26,27].

## ACKNOWLEDGMENTS

This work was performed under INTAS Grant No. 03-51-5448. O.V.Ya. and R.M.K. acknowledge financial support from NASU under Grant No. 10/07-H-32. We also thank Dr. I. Gerus (Institute of Petrol and Biochemistry of NASU, Kyiv, Ukraine) for providing us with the fluorinated polyimide.

[1] T. J. Sluckin and A. Poniewierski, in *Fluid Interfacial Phenomena*, edited by C. A. Croxton (Wiley, Chichester, U.K., 1986), Chap. 5, pp. 215–253.
[2] B. Jérôme, Rep. Prog. Phys. **54**, 391 (1991).
[3] G. Barbero and G. Durand, in *Liquid Crystals in Complex Geometries*, edited by G. P. Crawford and S. Žumer (Taylor & Francis, London, 1996), Chap. 2, pp. 21–52.
[4] H. V. Känel, J. D. Litster, J. Melngailis, and H. I. Smith, Phys. Rev. A **24**, 2713 (1981).
[5] B. Alkhairalla, H. Allinson, N. Boden, S. D. Evans, and J. R. Henderson, Phys. Rev. E **59**, 3033 (1999).
[6] P. Chiarelli, S. Faetti, and L. Fronzoni, J. Phys. (Paris) **44**, 1061 (1983).
[7] P. Chiarelli, S. Faetti, and L. Fronzoni, Phys. Lett. **101A**, 31 (1984).
[8] A. A. Sonin, A. Yethiraj, J. Bechhoefer, and B. J. Frisken, Phys. Rev. E **52**, 6260 (1995).
[9] T. Shioda, B. Wen, and C. Rosenblatt, Phys. Rev. E **67**, 041706 (2003).
[10] P. Pieranski and B. Jérôme, Phys. Rev. A **40**, 317 (1989).
[11] J. Bechhoefer, B. Jérôme, and P. Pieranski, Phys. Rev. A **41**, 3187 (1990).
[12] J. Bechhoefer, J.-L. Duvail, L. Masson, B. Jérôme, R. M. Hornreich, and P. Pieranski, Phys. Rev. Lett. **64**, 1911 (1990).
[13] J. Bechhoefer, B. Jérôme, and P. Pieranski, Phase Transitions **33**, 227 (1991).
[14] W. M. Gibbons, P. J. Shannon, S.-T. Sun, and B. J. Swetlin, Nature (London) **351**, 49 (1991).
[15] Z. Li, Liq. Cryst. **19**, 307 (1995).
[16] D. Andrienko, Y. Kurioz, Y. Reznikov, and Y. Reshetnyak, JETP **112**, 2045 (1997); Y. A. Reznikov and O. V. Yaroshchuk, in *Abstracts of OLC'95*, VI International Topical Meeting on Optics of Liquid Crystals, Le Touquet, France, 1995 (unpublished), p. 42.
[17] D. Andrienko, A. Dyadyusha, Y. Kurioz, V. Reshetnyak, and Y. Reznikov, Mol. Cryst. Liq. Cryst. Sci. Technol., Sect. A **321**, 299 (1998).
[18] L. Komitov, K. Ichimura, and A. Strigazzi, Liq. Cryst. **27**, 51 (2000).
[19] M. O'Neill and S. M. Kelly, J. Phys. D **33**, R67 (2000).
[20] V. G. Chigrinov, V. M. Kozenkov, and H. S. Kwok, in *Optical Applications in Photoaligning*, edited by L. Vicari (Institute of Physics, Bristol, U.K., 2003), pp. 201–244.
[21] J. L. Janning, Appl. Phys. Lett. **21**, 173 (1972).
[22] W. Urbach, M. Boix, and E. Guyon, Appl. Phys. Lett. **25**, 479 (1974).
[23] B. Jerome, M. Boix, and P. Pieranski, Europhys. Lett. **5**, 693 (1988).
[24] M. Monkade, M. Boix, and G. Durand, Europhys. Lett. **5**, 697 (1988).
[25] P. Chaudhari *et al.*, Nature (London) **411**, 56 (2001).
[26] O. Yaroshchuk, R. Kravchuk, A. Dobrovolskyy, L. Qui, and O. D. Lavrentovich, Liq. Cryst. **31**, 859 (2004).
[27] O. Yaroshchuk, R. Kravchuk, A. Dobrovolskyy, P.-C. Liu, and C.-D. Lee, J. Soc. Inf. Disp. **13**, 289 (2005).
[28] A. K. Sen and D. E. Sullivan, Phys. Rev. A **35**, 1391 (1987).
[29] V. Zhurin, H. Kaufman, and R. Robinson, Plasma Sources Sci. Technol. **8**, R1 (1999).
[30] B. H. Hwang, Y. M. Jo, D. S. Seo, S. J. Rho, D. K. Lee, and H. K. Baik, Jpn. J. Appl. Phys., Part 2 **41**, L654 (2002).
[31] Y. Galerne and P. Hubert, Eur. Phys. J. B **8**, 245 (1999).
[32] J. G. Fonseca, J. Hommet, and Y. Galerne, Appl. Phys. Lett. **82**, 58 (2003).
[33] E. Jang, H. Song, and S.-D. Lee, Jpn. J. Appl. Phys., Part 2 **45**, L1238 (2006).
[34] H. Akiyama and Y. Iimura, Jpn. J. Appl. Phys., Part 2 **40**, L765 (2001).
[35] S.-S. Lin and Y.-D. Lee, Jpn. J. Appl. Phys., Part 2 **45**, L708 (2006).
[36] M. Lu, Jpn. J. Appl. Phys., Part 1 **43**, 8156 (2004).
[37] C. Chen, P. J. Bos, J. Kim, and Q. Li, J. Appl. Phys. **99**, 123523 (2006).
[38] A. Rapini and M. Papoular, J. Phys. (Paris), Colloq. **30**, C4-54 (1969).
[39] P. G. de Gennes and J. Prost, *The Physics of Liquid Crystals* (Clarendon, Oxford, 1993).
[40] J. D. Parsons, Phys. Rev. Lett. **41**, 877 (1978).
[41] W. E. McMullen, Phys. Rev. A **38**, 6384 (1988).
[42] P. I. C. Teixeira and T. J. Sluckin, J. Chem. Phys. **97**, 1490 (1992).
[43] M. A. Osipov and T. J. Sluckin, J. Phys. II **3**, 793 (1993).
[44] F. N. Braun, T. J. Sluckin, E. Velasco, and L. Mederos, Phys. Rev. E **53**, 706 (1996).
[45] L. Faget, S. Lamarque-Forget, P. Martinot-Lagarde, P. Auroy, and I. Dozov, Phys. Rev. E **74**, 050701(R) (2006).
[46] G. Barbero, P. Jägemalm, and A. K. Zvezdin, Phys. Rev. E **64**, 021703 (2001).
[47] A. D. Kiselev, V. G. Chigrinov, and D. D. Huang, Phys. Rev. E

**72**, 061703 (2005).
[48] D.-H. Chung, T. Fukuda, Y. Takanishi, K. Ishikawa, H. Matsuda, H. Takezoe, and M. A. Osipov, J. Appl. Phys. **92**, 1841 (2002).
[49] Z. Huang and C. Rosenblatt, Appl. Phys. Lett. **86**, 011908 (2005).
[50] J. Chen, D. L. Johnson, P. J. Bos, X. Wang, and J. L. West, Phys. Rev. E **54**, 1599 (1996).
[51] A. D. Kiselev, J. Phys.: Condens. Matter **14**, 13417 (2002).
[52] O. V. Yaroshchuk, A. D. Kiselev, Y. Zakrevskyy, T. Bidna, J. Kelly, L.-C. Chien, and J. Lindau, Phys. Rev. E **68**, 011803 (2003).